SAND2018-10526C

Thermo-Hydro-Mechanical Evaluation of Critical Mass in Repository Far-Field

Alex Salazar,*[1] Massimiliano Fratoni[2]
[1]Sandia National Laboratories, United States
[2] University of California, Berkeley, United States

Abstract

The evaluation of post-closure safety for a repository for spent nuclear fuel (SNF) includes feature, event, and process (FEP) and scenario screening of potentially relevant phenomena. This study examines the potential consequences of a low-probability criticality FEP; specifically, the impact of a critical mass formation in the far-field in a scenario where canisters are extensively compromised, fuel is dissolved, and fissile nuclides are re-concentrated. If reactivity feedback is insufficient to bring the system to a subcritical state and heat transfer to the surrounding host rock is inadequate, the surrounding rock is liable to degrade via thermal creep. Based on past studies, the probability of an autocatalytic, or explosive, criticality event from SNF is considered negligible. Therefore, to evaluate the potential for mechanical failure with a long-term release of energy, this study evaluates a critical deposition in host rock by coupling a neutronics analysis and thermo-hydrological simulation of heat and mass transport. Using plausible uranium precipitate compositions, critical configurations are obtained based on a spherical geometry in either a homogeneous or repeated laminar configuration of rock, UO_2 precipitate, and pore fluid. These critical geometries are obtained per given mass of uranium via a static neutronics analysis assuming a water-saturated formation surrounded by successive layers of shale and granite. The TOUGH2 code is used to evaluate the saturation in the porous medium with evolving temperature based on the fission source term. Reactivity feedback models are obtained to account for the effects of Doppler broadening and the arriving plume of uranium, which are then incorporated into a quasi-steady-state heat transfer model to determine the lumped system temperature over time. These results are applied numerically in a thermal creep model to determine the period post-formation when mechanical deformation of the host rock is indicative of failure. Results are found to be sensitive to the source term of fissile material, however, in a direct disposal scenario, the necessary concentration of critical mass would not likely be feasible. Ultimately, given the conservative nature of the assumptions employed in the study, the conditions leading to failure via thermal creep are improbable.

Sandia National Laboratories is a multimission laboratory managed and operated by National Technology & Engineering Solutions of Sandia, LLC, a wholly owned subsidiary of Honeywell International Inc., for the U.S. Department of Energy's National Nuclear Security Administration under contract DE-NA0003525.

Introduction

A repository for spent nuclear fuel (SNF) relies on engineered and natural barriers to reduce the post-closure risk of radionuclide releases to the biosphere over long periods of time. Post-closure repository analyses include feature, event, and process (FEP) analysis and scenario development to identify and screen potentially relevant phenomena.[1] Criticality FEPs (in-package, near-field, and far-field) are typically screened out on the basis of low probability.[2] This study examines the consequences of a hypothetical far-field criticality scenario, independent of the low probability screening.

In a post-closure scenario wherein multiple canisters are extensively compromised, the dissolution, transport, and re-concentration of fissile nuclides could lead to a critical mass formation that may pose a threat to the material integrity of the engineered and/or natural barriers. In particular, if heat transfer to the surrounding host rock is inadequate and high temperatures persist over long periods of time, the release of energy from sustained chain reactions may eventually degrade the surrounding rock and introduce a pathway for fission products to the biosphere. To evaluate the potential for host rock failure given a long-term release of energy, this study evaluates the consequences of a critical deposition by coupling a neutronics analysis and a simulation of unsaturated heat and mass transport. In particular, thermal creep is proposed as a time- and temperature-dependent failure metric as opposed to the high-energy, autocatalytic scenarios evaluated in past studies.[3]

Critical dimensions of plausible precipitate enrichments are obtained from a parametric study using the Monte Carlo N-Particle (MCNP) transport code based on the void space available to water and heavy metal.[4] The behavior of porous heat and groundwater transport in the critical configuration of uranium, water, and rock is assessed using the TOUGH2 code. The results of fluid content and density over time are used to guide an integrated neutronics evaluation that measures the simultaneous reactivity feedback effects of Doppler broadening and the loss of moderator. Feedback coefficients are employed in a lumped capacitance heat transfer analysis that models the critical mass and bedrock at quasi-steady-state to probe the evolution of system temperature over time. These time-dependent results are then applied to a creep strain model to evaluate total system deformation.

Methodology

Scenario for mass transport

As noted above, criticality FEPs are typically screened out because of the very low probability of out-of-package fissile material attaining a critical configuration. However, if multiple waste canisters in the repository tunnels undergo early failure, radionuclides from the fuel may undergo dissolution, groundwater transport in fractures, and subsequent re-concentration in a reducing region of the far-field. Such conditions could be provided by sedimentary deposits like shale and would allow for uranium, mobilized as the uranyl anion, to drop out of solution as a precipitate in the available void space. The criticality analysis examines potential far-field consequences, with these hypothetical low-probability conditions assumed as a precursor.

A conservative transport analysis was conducted for an abstracted repository grid containing the approximately 70,000 MTU of SNF in the current United States inventory.[5] The compositions and mass loadings of BWR and PWR SNF were averaged to create uniform canister radionuclide inventories. An average canister was determined to hold 1.880 MTU of heavy metal, or about 7900 moles of original uranium, which required the repository to hold 37,249 canisters to accommodate the source term.

This study assumed a superposition of all mass flux contributions from individual emplacements in the repository at a common point in the far-field by way of advective transport in granitic fractures. No concentration limitations from upstream canister flow or any other inter-canister mass transport limitations were allowed to limit the flux of radionuclides. Each emplacement consisted of a canister and surrounding bentonite buffer modeled according to a spherical geometry that preserved interfacial surface areas to model diffusive mass transport upon dissolution after a common 1000-year failure period. The analysis employed a statistical sampling technique to acknowledge the full range of uncertainty in the range of sorption, solubility, and diffusion parameters in the granitic geology. Results indicated maximum accumulations occurring on the order of a metric ton after several million years. Steady-state enrichment levels in the precipitate were found to lie around 1.5 wt%, with enrichments as high as 6 wt% occurring in upper bound (90% quantile) behavior due to highly mobile transuranics serving as uranium precursors. To limit the scope of this study, uranium-dominated depositions will be considered at 1.5 wt%, 2 wt%, and 3 wt%, which are held to be most indicative of the direct disposal context.

Neutron transport

The far-field precipitate is modeled as a sphere in one of two geometries: 1) a homogeneous mixture of rock, UO_2, water, and air, or 2) a heterogeneous arrangement of those components in repeating slab units to emulate natural rock fractures (see Figure 1). The sphere is surrounded by a one-meter thick layer of saturated shale at 10% effective porosity, which represents the sedimentary rock needed to provide a reducing environment. It also serves as a neutron reflector to conservatively reduce the critical mass. The shale envelope is surrounded by a ten-meter thick layer of saturated granitic host rock at 1% effective porosity. In the neutronics evaluation, the granite is modeled as being surrounded by void, as the total neutron collision density is expected to be small. However, when evaluating heat and mass transport, the boundary is modeled as an infinite extent of granite.

The critical configurations of the system are determined via a parametric analysis in MCNP based on altering the volumetric fractions of total saturated void (VVF) and heavy metal (HMVF) up to 36 vol%. The HMVF cannot be larger than VVF, and the difference between the two parameters is called the fluid volume fraction (FVF). The VVF is controlled by the aperture (b) in the fractured geometry and by the typical porosity in the homogeneous host rock. The radius of the sphere (r_c) is adjusted to accommodate the mass of UO_2 being analyzed, which is based on the full theoretical density of 10.95 g/cm^3 as a measure of conservatism. The density of pore water is assumed to be 1.005 g/cm^3 based on an assumed hydrostatic pressure of 15 MPa, while that of air is 0.00177 g/cm^3.

The rock assumed in the homogeneous mixture is sandstone, which is modeled as pure SiO_2, whereas the rock slabs in the fractured geometry have the same shale composition as the reflector. A solid density of 2.8 g/cm^3 is modeled for shale, 2.65 g/cm^3 for sandstone, and 2.75 g/cm^3 for granite. The Si(SiO_2) S[α,β] thermal scattering library is used for both shale and granite, whereas the U(UO_2) library is used for cells with U and H(H_2O) for water.

Figure 1 : Model of critical mass of radius r_c and surrounding rock (not to scale) employed in the neutronics analysis, where *b* is the aperture of the fractured geometry.

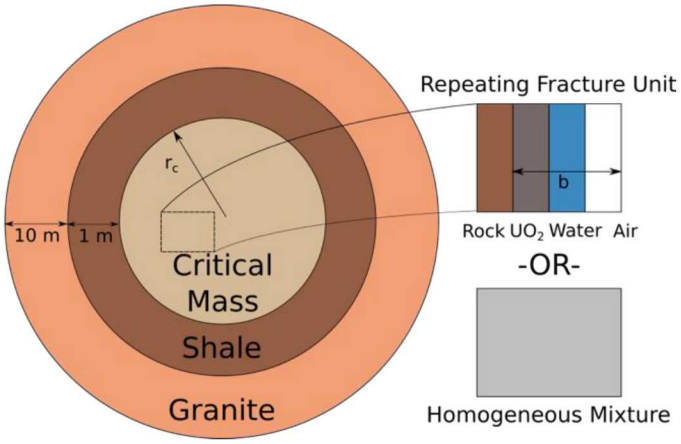

Unsaturated heat and mass transfer

The TOUGH2 integrated finite difference code with the water/air equation-of-state module (EOS3) was employed to analyze the flow of pore fluid and heat from the critical mass to the surrounding rock.[6] The MCNP cells with their associated surface areas, volumes, and porosities and are mirrored in the problem setup, although each region is discretized into fifteen spherical annuli to analyze spatial variation. Furthermore, an infinite region of granite is modeled at the boundary with a very low saturation level of 0.1% to artificially amplify the capillary suction of water from the system. Dry conditions were chosen to observe a minimum saturation in the precipitate and to evaluate smoother behavior as the boiling point of water is exceeded. The hydrostatic pressure is assumed to lie at 15 MPa, where the phase transition of water from liquid to gas occurs at T_{BP}=342.155°C.

The thermal conductivity (*k*) for the rock formations are provided for both wet and dry conditions, whereas a single value is used for the precipitate to be representative of high grade ore. The critical region is modeled as being more pervious than the shale and granite, with a permeability of 10^{-15} m^2 (≈1 milli-Darcy) compared to 10^{-18} m^2 (≈1 µD). This higher value is chosen to reflect the highly fractured nature of the rock needed to accommodate the necessary amount of UO_2 for a critical mass. Permeability is treated isotropically and gravitational effects are eliminated. The van Genuchten-Mualem model is employed to model the relative permeability (K_r) of both water and air in the pore space, using a fitting parameter of λ=0.5.[7] The residual saturations of water and air are 5% and 1%, respectively. For capillary pressure, van Genuchten's function is employed with the previous λ fitting parameter and P_0=200 kPa. In this relationship, the residual water saturation is modeled as 1%. In this study, these functions are applied globally to all regions in the model. Since the shale composition includes smectite clay, the tortuosity factor for binary diffusion is set at τ =1, whereas for others it is kept as zero.

The spatial dependence of the fission source term within the precipitate is obtained using the CINDER depletion module in MCNP. Initial power outputs of 0.1 and 1 kW_t were employed to evaluate the general spatial profile, which conformed to the functional form of a truncated Gaussian curve in the radial direction. This functional form was then used to test total thermal outputs (q_{opt}) needed for

the average temperature of the critical mass to reach the phase transition temperature at steady-state. This was done to ensure a full evaluation of two-phase flow conditions.

Table 1: Properties for materials relevant to the study, where the porosity of the precipitate is determined by the fluid volume fraction needed for criticality. Sandstone is used as the rock component of the homogeneous geometry.

Material	Permeability [m^2]	Thermal Conductivity [W/m-K]		c_p [J/kg-K]	ρ [g/cm^3]	Tortuosity Factor	Porosity [%]
		Dry	Wet				
Precipitate	10^{-15}	varies				0	FVF (1% min)
UO_2	-	7	7	260	10.95	-	-
Shale	10^{-18}	1.8	2.9	795	2.8	1	10
Granite	10^{-18}	2.79	3.2	840	2.75	0	1
Sandstone	10^{-15}	1.9	3.8	825	2.65	0	10

Doppler feedback in heated and unsaturated critical mass

The TOUGH2 results are used to guide a neutronics evaluation of reactivity changes given evolving average temperature and saturation in the discrete regions of the system. Since the thermohydrological simulation only reaches the phase transition temperature, a simple thermal resistance model is used to extend the temperature to a maximum average of 1250°C, which represents the melting point of rock. In this treatment, the fine-scale behavior of the flow and thermal expansion of the pore gas (both vapor and air) is highly simplified, as the gaseous components are not expected to influence neutron absorption substantially.

The On-the-Fly Doppler Broadening (OTFDB) code is used to model for the effects of increasing temperature on neutron absorption.[8] The ENDF-B/VII.1 libraries were used to create functional expansions for all nuclides in the problem (except neon) that could be directly read during the MCNP simulation. High-order interpolations were made in 10°C intervals from 0°C to 1300°C based on energy grids with 100°C intervals. Absorption cross sections are modified when collisions are scored in a particular cell using the specified average temperature.

The initial temperature of the system is set at 20.45°C to align with the cross section libraries employed in the critical mass assessment; the effect of the geothermal gradient is therefore neglected. The densities of the water and air in the pores are modified based on the results of the TOUGH2 simulation. The individual solid densities of the porous materials and metals are held constant with temperature, whereas the bulk solids are modified to account for the effects of evolving pore fluid densities.

Quasi-steady-state lumped capacitance model

Given the various reactivity feedback mechanisms taking place in the system, an analysis is employed that integrates a reactivity balance in a system of equations involving point depletion. A lumped capacitance approach is employed to model heat transfer between the critical mass and the surrounding rock, which assumes that radial variation of temperature in the precipitate is negligible.

The energy balance consists of an energy storage component with precipitate mass M and specific heat C_p and a convective component with heat transfer coefficient h and surface area A, as shown in Equation (1).

$$Q(t) = MC_p\dot{\Delta T}(t) - hA\Delta T(t) \tag{1}$$

Heat transfer correlations exist for fluid flow around spheres in porous media, both for natural and forced convection. However, the use of lumped capacitance restricts the use of these correlations, and instead a fundamental limit on h is employed based on the Biot number: Bi<0.1. This implies a maximum value of h based on the effective thermal conductivity and radius of the critical mass, as shown in Equation (2).

$$h = \frac{3k}{10r_c} \tag{2}$$

The power generated from fission is governed by the scalar neutron flux ϕ, fission cross sections σ_f, and useable energy released per fission E_f from all fissile nuclides, as shown in Equation (3).

$$P(t) = \phi(t)\left[E_f^{25}\sigma_f^{25}n_{25}(t) + E_f^{49}\sigma_f^{49}n_{49}(t)\right] \tag{3}$$

A point depletion is applied to determine the critical sphere composition of three nuclides over time: fissile U-235 (Equation (4)) and Pu-239 (Equation (5)), and fertile U-238 (Equation (6)). In these expressions, σ_c represents the cross section for neutron capture, λ is the decay constant, and $\dot{S}$ is the source term from the repository plume in mol/yr.

$$\dot{n}_{25}(t) = \dot{S}_{25} + \lambda_{49}n_{49}(t) + \phi(t)\left[-\sigma_c^{25}n_{25}(t) - \sigma_f^{25}n_{25}(t)\right] \tag{4}$$

$$\dot{n}_{49}(t) = \dot{S}_{49} - \lambda_{49}n_{49}(t) + \phi(t)\left[\sigma_c^{28}n_{28}(t) - \sigma_c^{49}n_{49}(t) - \sigma_f^{49}n_{49}(t)\right] \tag{5}$$

$$\dot{n}_{28}(t) = \dot{S}_{28} - \sigma_c^{28}n_{28}(t)\phi(t) \tag{6}$$

The quasi-steady-state (QSS) approach to consequence analysis assumes that fission power generation and heat dissipation from the critical system are in a relative steady state, and that the system remains critical until competing reactivity feedback mechanisms result in subcriticality.[9] Therefore, given a gradual release of energy, Equations (1) and (3) are equated to solve for the scalar flux (Equation (7)), which removes nonlinearity from the system of equations.

$$\phi(t) = \frac{MC_p\dot{\Delta T}(t) + hA\Delta T(t)}{N_A\left[E_f^{25}\sigma_f^{25}n_{25}(t) + E_f^{49}\sigma_f^{49}n_{49}(t)\right]} \tag{7}$$

The study assumes that all reactivity feedback mechanisms balance to eventually drive the system to subcriticality. Therefore, Equations (4) through (6) are coupled with the reactivity balance in Equation (8) to form N+1 total equations, where α_T is the temperature feedback coefficient [#/°C], α_{25} is the feedback coefficient for the evolving inventory of U-235 [#/mol], α_{28} is the feedback coefficient for the poisonous effect of the U-238 influx, and α_R is the feedback coefficient due to thermal expansion. α_{25} is obtained through two-dimensional interpolations of the criticality data for each VVF, HMVF coordinate for a given enrichment to simulate the addition of enriched uranium to an empty void space. As the void space fills, this coefficient is positive until the addition of heavy metal results in undermoderated conditions and a negative value; therefore, the term is modeled as a parabolic function of the addition of U-235: $n_{25}(t) - n_{25}^0$. α_{28} is obtained through interpolation in a similar manner albeit across multiple enrichments for a given coordinate to simulate the effect of adding pure

U-238 (in UO_2) to the void space. This value is consistently negative due to fertile absorption and can be modeled as a constant, negative value. The term $f_R(\Delta T)$ represents the change in the radius of the critical mass with respect to temperature. Altogether, it should be noted that the magnitude of the thermal expansion term is relatively negligible compared to the other terms in the equation. Finally, α_T is obtained through the neutronics analysis integrating the thermohydrological results. No feedback coefficient is included for saturation effects because a major assumption of the study is that temperature and saturation cannot be decoupled in the steady-state porous medium, i.e. α_T includes desaturation effects.

$$\alpha_T(T)\frac{\partial \Delta T(t)}{\partial t} + \alpha_{25}\left[n_{25}(t) - n_{25}^0\right]\frac{\partial n_{25}(t)}{\partial t} + \alpha_{28}\frac{\partial n_{28}(t)}{\partial t} + \alpha_R(\Delta T) f_R(\Delta T)\frac{\partial \Delta T(t)}{\partial t} = 0 \qquad (8)$$

Mechanical failure metric

After the coupled behavior of temperature over time is evaluated given the various feedback mechanisms, another model must be applied to quantify the impact of the fission energy release on the material integrity of the natural barriers. Among other possible failure mechanisms, creep is proposed as a time- and temperature-dependent mechanical deformation process readily quantifiable from the QSS results. This phenomenon occurs at a constant applied stress below the ultimate tensile stress of the host rock. As temperatures become significantly high (above 150°C but below the melting point) equilibrium vacancies form in the constituent minerals, which are then mobilized through grain boundary diffusion or dislocation climb. Although creep can be separated into primary, secondary, and tertiary regimes, the most relevant to this scenario is the steady-state character of secondary creep. Furthermore, although irradiation creep is physically applicable to the system, only thermal creep is acknowledged to remain within the thermohydrological scope.

The time-integrated strain (ε) from thermal creep is described in Equation (9), where σ is the applied stress of 30 MPa (representative of the overburden pressure), G is the shear modulus of 10 GPa, n is the stress exponent of 3.5, Q is the activation energy of 20 kJ/mol, R is the gas constant, and T is the QSS temperature in centigrade. The constant A is chosen as 2252 s^{-1} so that the strain rate is equal to 10^{-9} s^{-1} at 150°C. This strain rate is considered to be an upper bound choice for a geological context. There is no material strain below 150°C since the temperatures would not be high enough to induce plastic deformation. A 1.5% plastic deformation metric is employed to evaluate system failure, as this would indicate an increase in permeability to volatile fission products.

$$\epsilon = \begin{cases} \int_0^t A\left(\frac{\sigma}{G}\right)^n e^{-Q/R[T(\tau)+273.15]}d\tau & 150°C \le T < 1250°C \\ 0 & T < 150°C \end{cases} \qquad (9)$$

Results

Minimum critical masses for the various uranium enrichments in both homogeneous and fractured geometries are shown in Table 2. The fracture aperture was chosen to be optimal for attaining a minimum critical mass at 1 cm for the 1.5 and 2 wt% enrichments, whereas 0.5 cm was optimal for the 3 wt% depositions. The 1.5 wt% enrichment level, which is indicative of the steady-state fissile content in the precipitate, does not reach criticality in the homogeneous configuration within the scope of VVF and HMVF, whereas in the fractured geometry, large dimensions and masses exceeding 100 MTU are

required. This disqualifies the steady-state enrichment level as a probable accumulation. In general, smaller critical masses are attainable in higher-enriched precipitates, yet as the critical radius decreases, less realistic void volume fractions are required. Therefore, minimum critical masses would likely deposit in highly porous or fractured zones in the far-field.

The critical dimensions are analyzed in TOUGH2 to determine power levels (q_{opt}) leading to minimal saturation levels. The thermal output required for the precipitates to boil pore water increases linearly with the critical radius (and mass). These power levels vary between 0.1 and 1 kW_t, which shows convergence with the values assumed in the CINDER depletion study when determining the spatial fission power profiles. The reduction in reactivity when the pore water is removed from the critical mass (D_M) is usually stronger for smaller critical masses and the homogeneous configuration. The fractured geometry is less affected by the loss of moderator due to spatial self-shielding of resonance energy neutrons and some moderating character in the rock slabs.

Table 2: Results for the critical dimensions of certain masses and enrichments of the far-field precipitate, along with thermal outputs (q_{opt}) needed to bring the average temperature of the system to the phase transition temperature. The temperature defect (D_T) when heating the precipitate to an average temperature of 342.155°C is included.

Geometry	Enr. [wt%]	Mass [MTU]	r_c [cm]	VVF	HMVF	q_{opt} [W_t]	D_T
Homogeneous	2	5	105.6	0.3375	0.105	309.77	-1.85099
		10	133.3	0.3075	0.1045	328.32	-1.70324
		100	301.8	0.2565	0.09	435.94	-1.38623
	3	1	69.1	0.2965	0.075	280.08	-1.79588
		5	127.3	0.2005	0.06	324.61	-1.5628
		10	160.8	0.1810	0.0595	345.02	-1.41846
Fractured	1.5 b=1 cm	100	254.6	0.2710	0.1499	406.25	-1.16179
		500	435.4	0.2544	0.1498	526.86	-1.16179
		1000	548.4	0.2528	0.15	608.50	-1.16901
	2 b=1 cm	5	101.0	0.2229	0.12	306.05	-1.57402
		10	127.7	0.1905	0.1188	324.61	-1.42132
		100	286.7	0.1424	0.105	426.66	-1.0382
	3 b=0.5 cm	0.1	50.9	0.2925	0.094	259.67	-1.91903
		1	65.3	0.2018	0.089	276.37	-1.66114
		5	118.1	0.0930	0.075	317.19	-1.22101
		10	150.0	0.0738	0.07325	339.45	-1.0189

The behavior of temperature and saturation (S_l) over time is shown in Figure 2 using the critical dimensions of the 2 wt% homogeneous precipitate as examples. As the system begins heating, the average temperatures rise steadily while the system remains mostly at full saturation. This rise in temperature is stronger for smaller precipitates, which appear to reach what vaguely resembles a steady-state. After a short period near steady-state, around ten years, dT/dt increases substantially, and the temperature increases until the final steady-state level is reached. This rise is caused by the loss of pore water due to capillary suction effects, which reduces the thermal conductivity of the sphere.

The saturation begins to decrease around 500 years into the simulation when average temperatures begin to exceed approximately 100°C. The fall from S_l=1 to 0 over time is exponential (linear on the log-scale plot) between 100°C and the saturation temperature. A linear, inverse relationship between temperature and saturation is highlighted in Figure 3 for discrete regions in the critical mass, where the threshold temperature for accelerated desaturation appears to lie between 75°C and 100°C. It is clear that per given temperature, the corresponding saturation is lowest at the surface of the sphere, although these small differences are less noticeable for larger masses.

Figure 2: The spatially-averaged behavior of temperature (black, left axis) and saturation (blue, right axis) over time in the TOUGH2 simulation of the 2 wt% homogeneous critical masses, assuming a dry environment at 0.1% saturation.

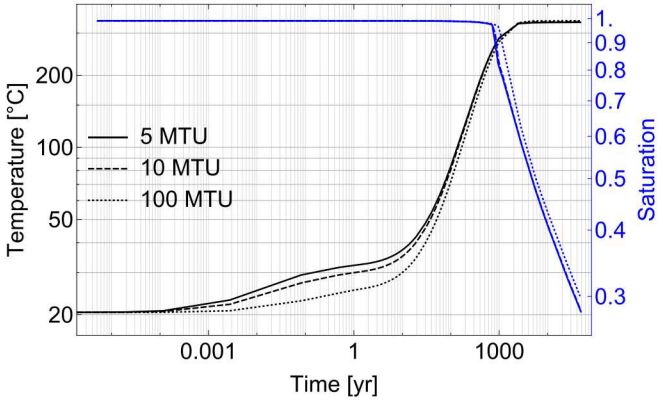

Figure 3: The behavior of saturation with temperature for each discrete region of the 5 MTU 2 wt% homogeneous critical mass ("CRM") as steady-state is reached for a dry environment at 0.1% saturation. The regions are numbered from the core outwards.

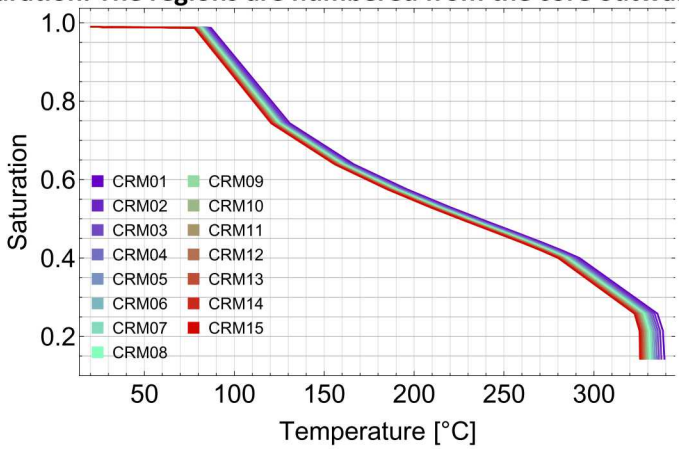

The temperature and saturation results from TOUGH2 are used to devise an integrated neutronics analysis to analyzed coupled feedback from Doppler broadening and the loss of moderator, and some results are shown in Figure 4. Although the effects from Doppler broadening are not very noticeable when the critical mass contains most of its water, the increase in temperature eventually leads to a reduction in reactivity. This reduction takes place when desaturation occurs at a threshold temperature of 100°C, and this is closely followed by a discontinuity in behavior around the boiling point when liquid is completely evacuated from the pore space. After the boiling point, the reactivity decreases monotonically but at a more gradual and steadier rate, where changes come purely through

Doppler broadening in the heated fuel and, to a presumably lesser extent, the rock. The decreases in ρ are more significant for smaller critical masses because of greater neutron leakage. Also, while not shown, the drops in reactivity are weaker for more highly enriched precipitate compositions because fewer neutrons are absorbed in the resonances of fertile U-238.

The temperature defect D_T is defined as the integrated change in reactivity when the critical mass is heated between a certain temperature range. In Table 2, D_T is observed to be consistently stronger for the homogeneous configuration compared to the fractured. The fluid volume fraction in the latter configuration is usually lower per given mass of heavy metal, so this behavior is expected from less neutrons being moderated to resonance energies. Nonetheless, general behavior is similar between the two geometries. Per given mass, D_T decreases with enrichment because a higher concentration of fissile material allows for less neutrons to be absorbed in the fertile material. Per given enrichment, the defect is usually stronger for smaller critical masses, with this discrepancy evidently stronger at higher enrichments. Given these dependencies, the 5 MTU, 2 wt% homogeneous case is highlighted as an example for further results, where the spherical surface area and volume of interest are 14.01 m^2 and 4.932 m^3, respectively. The volume available to fluid in this critical mass is 1.147 m^3.

Figure 4: Behavior of reactivity per average temperature in the 2 wt% precipitate in the (a) homogeneous and (b) fractured configurations.

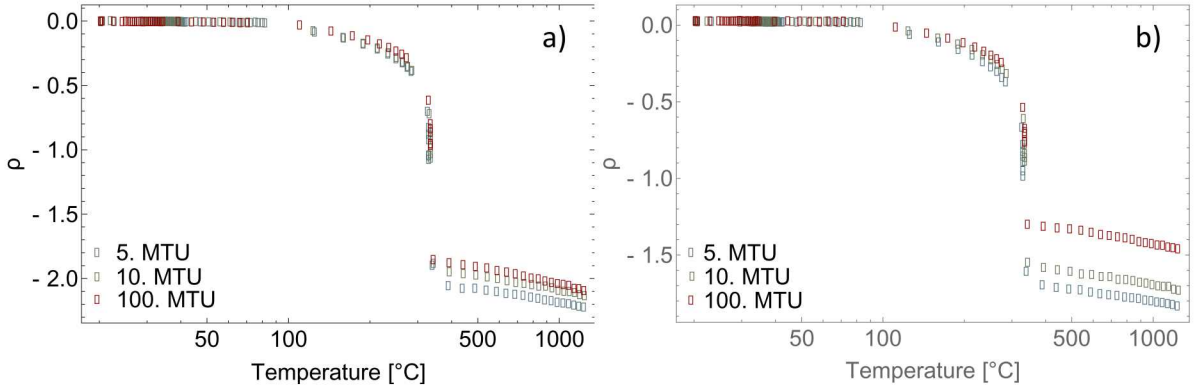

Given the discontinuous behavior around the boiling point, in order to carry α_T over to the QSS analysis, the feedback coefficients $\left(\frac{\partial \rho}{\partial T}\right)$ for each critical mass are obtained through two functional forms for regression of ρ(T):

1. A piecewise function employing an exponential term and a power law with individual fitting terms α_0, α_1, α_2, α_3, and x: $\rho(T) = \begin{cases} \alpha_0 - \alpha_1 e^{-\alpha_2 T + \alpha_3} & T \leq T_{BP} \\ \alpha_0 + \frac{\alpha_1}{T^x} & T > T_{BP} \end{cases}$

2. A Gaussian-type function with fitting terms α_0, α_1, μ, and σ: $\rho(T) = \alpha_0 + \frac{\alpha_1}{\sqrt{2\pi\sigma^2}} e^{-\frac{(T-\mu)^2}{2\sigma^2}}$

The Gaussian fit has the advantage of modeling behavior in a continuous manner, although the magnitude of the feedback coefficient is underestimated leading up to the phase transition and then overestimated when the system is dry. The piecewise fit has the advantage of more accurately fitting system behavior, therefore retaining the discontinuity observed in the results.

The feedback coefficients are applied to the system of equations in the lumped capacitance model by first parametrizing the source term of uranium. The source term of plutonium is kept at zero, and $\dot{S}_{25}$ and $\dot{S}_{28}$ are kept proportional to the enrichment of the precipitate. In Figure 5, it is shown that a maximum temperature change is achieved before decreasing to an eventually constant value of ΔT, and that the Gaussian fit for α_T leads to the highest temperature evolution due to the overestimation of feedback when the system becomes dry. The decrease in ΔT is caused by the system becoming undermoderated from the amount of precipitate accumulating in the pore space, while the steady level is caused by the pore space becoming completely filled.

Higher source terms lead to temperature peaks occurring sooner in time, and at least 1 mmol/yr of uranium is needed for maximal ΔT to be observed within the temporal scope of the study. This would correspond to an entire canister's worth of heavy metal being re-concentrated at a single location in a time span of about 8 million years. For reference, a total uranium arrival rate of 0.0055 mmol/yr was observed in the transport analysis of ref. [5], which employed very conservative assumptions to purposefully overestimate the mass of heavy metal precipitating in the far-field rock from an entire repository. To cite a natural analog, uranium mobilized in the fractures of volcanic tuff at the Nopal I deposit of Peña Blanca are observed in concentrations between 51 μM and 32 mM,[10] which exceed the upper bound of solubility used in the transport study. Uranium dissolution rates were observed to lie at approximately 1 ppb per day or about 2 mmol/m^3/yr.[11] If the maximal Peña Blanca concentrations could be attained for the fuel of each SNF emplacement in a granitic environment, groundwater velocities of 10 m/yr and above would allow for the 1 mmol/yr threshold to be achievable in the pore volume depending on the level of radionuclide retardation in the fractures. However, the necessary solubility limits would likely require considerable degradation of both the fuel and bentonite buffer.

Figure 5: The temperature change over time in the 5 MTU 2 wt% homogeneous critical mass as parametrized by the source term of uranium (in mmol/yr) for piecewise (solid) and Gaussian (dashed) fits of α_T.

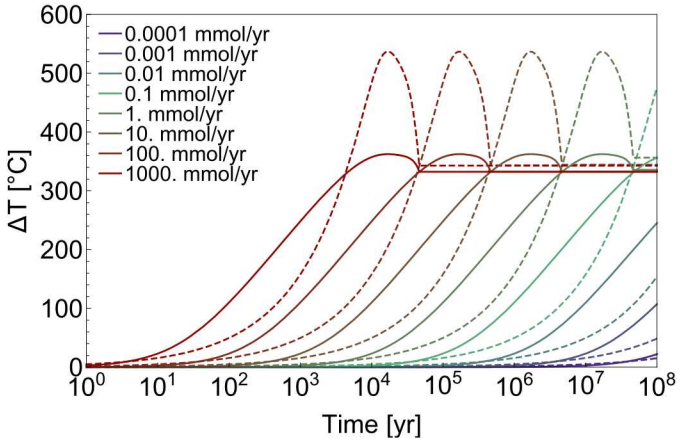

Next, the system of equations was parameterized based on modifying the value of $\dot{S}_{49}$, where $\dot{S}_{25} + \dot{S}_{28}$ was maintained at 0.0055 mmol/yr. In this scenario, Pu-239 arriving from the repository (as plutonium oxide) is assumed to augment the fission power output and the amount of U-235 generated through precursor decay, although positive feedback effects are limited to U-235 generation only. It should be noted that plutonium was excluded from the compositional calculations for the precipitate

due to relatively low quantities in the SNF; results for lower $\dot{S}_{49}$ are therefore considered to be most relevant to the direct disposal scenario.

In Figure 6, it is shown that for small values of $\dot{S}_{49}$ that begin to surpass $\dot{S}_U$, the temperature begins to rise earlier in time and reach a steady level, which is caused by decay contributions to the mass of U-235 and positive feedback from α_{25}. This is followed by a rise in ΔT caused by the original source of uranium. For the piecewise regression, a preliminary rise in the flux is observed for small $\dot{S}_{49}$ as Pu-239 begins to decay significantly after $2{\cdot}10^4$ yr, which is followed by a decrease until the original uranium source term can raise the flux again. The Gaussian regression shows a monotonic decrease until the $\dot{S}_U$ contributions are realized.

As $\dot{S}_{49}$ becomes much larger than $\dot{S}_U$, the original uranium plume has diminishing effect on reactivity, and positive feedback is directly imparted by the plutonium contributions. While not shown, increasing the plutonium influx increases the maximum flux, and a steady-state flux is attained after 200,000 years for $\dot{S}_{49} \leq 10^{-2}\frac{mol}{yr}$. When radiogenic U-235 becomes sufficiently large at $\dot{S}_{49} \geq 10^{-1}\frac{mol}{yr}$, the system becomes undermoderated, which results in subcriticality. Overall, these results and those of the other parameterization confirm the maximum temperatures that would be expected if the source of uranium was larger.

Figure 6: The temperature change over time in the 5 MTU 2 wt% homogeneous critical mass as parametrized by the source term of Pu-239 (in mmol/yr) for piecewise (solid) and Gaussian (dashed) fits of α_T.

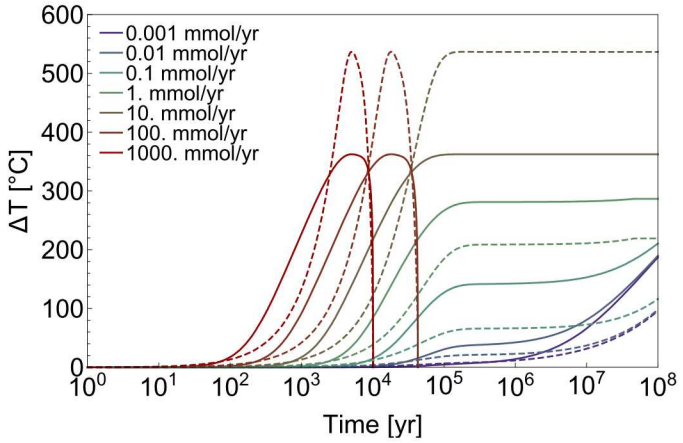

The integrated strain is shown in Figure 7 based on elevated source terms of enriched uranium from Figure 5. Only the results related to the Gaussian regression can be resolved on the plot, and the dashed line convention is maintained. It can be seen that higher $\dot{S}_U$ do not relate to higher integrated strain levels. Since creep is a time-dependent process, and larger source terms lead to temperature rises that occur earlier post-formation over shorter periods, there is not enough time for the system to appreciably deform. When the arrival rate of uranium is lower, the temperature rises over a more extended period of time, which allows for much more creep deformation. If the uranium arrival rate is 1 mmol/yr, the failure metric can be met around 10^7 yr. From these results, it appears there is an optimal arrival rate for meeting a high temperature and high strain while not being too unreasonably large from the nuclide transport perspective. The results for 10^{-3} mmol/yr, which are roughly similar

to the magnitude of the original transport results, do not resolve on the plot and are therefore not liable to result in creep failure over the temporal scope of the investigation.

Figure 7: The integrated creep strain over time in the 5 MTU 2 wt% homogeneous critical mass as parametrized by the source term of uranium (in mmol/yr) for a Gaussian fit of α_T.

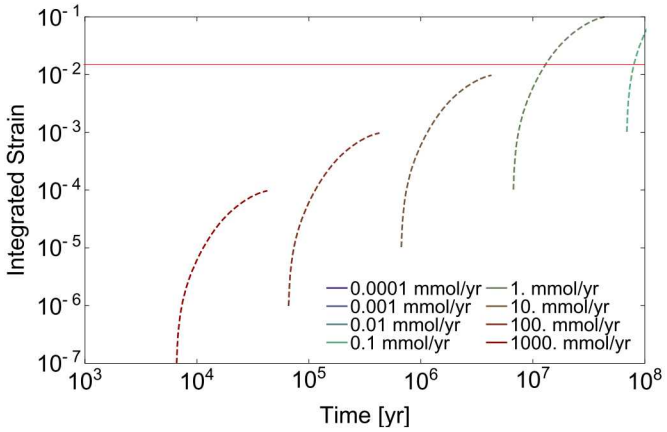

Figure 8 shows the results of integrated strain for various plutonium arrival rates, where the largest source terms exhibit low strain due to short durations of creep-relevant temperatures. However, an optimal value of $\dot{S}_{49}$ is found at 10 mmol/yr, where the strain increases monotonically all the way to failure at $4 \cdot 10^6$ yr. After this rate of influx, lower test values yield steady-state temperatures that are too low for creep to be applicable. Therefore, a window of applicability exists where a specific addition of fissile content from transuranics can lead to elevated and sustained temperatures needed for catastrophic creep deformation. However, it is very questionable whether such source terms of plutonium can be obtained in the direct disposal context, as about 0.5 wt% of the SNF is comprised of transuranic fissile material within a total fissile content of about 1.4 wt%.[5] The influx of plutonium cannot surpass that of uranium unless the geochemical conditions selectively mobilize plutonium over uranium; this was not the case at Peña Blanca, as plutonium mobility was observed to be three orders of magnitude less than uranium.[11]

Figure 8: The integrated creep strain over time in the 5 MTU 2 wt% homogeneous critical mass as parametrized by the source term of Pu-239 (in mmol/yr) for a Gaussian fit of α_T.

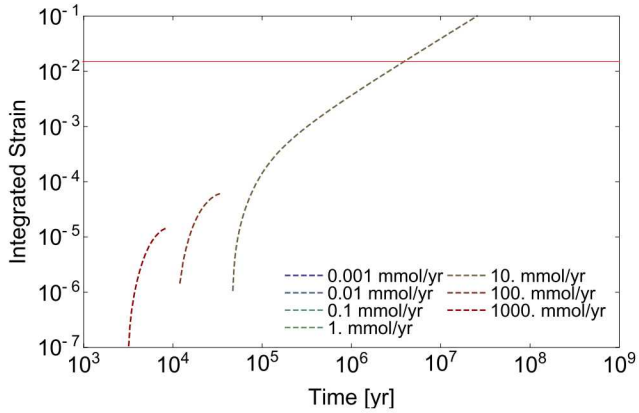

Conclusions

A criticality consequence analysis was presented for a hypothetical accumulation of uranium in the far-field subject to reactivity feedback from heating and the plume of heavy metal from the repository. It was shown that only under amplified source terms of fissile material can the critical mass be subject to failure via excessive plastic deformation from creep. In a direct disposal scenario, these parameters would not likely be feasible even with assumptions meant to amplify the quantity of heavy metal precipitation. Even if a failure mechanism has been introduced, given the hyper-conservative approach to each individual portion of the analysis, the failure of natural barriers from criticality is considered to be highly implausible.

Acknowledgements

The first author would like to acknowledge the support of the United States Nuclear Regulatory Commission (NRC) fellowship for his dissertation-related studies at the University of California, Berkeley.

Sandia National Laboratories is a multi-mission laboratory managed and operated by National Technology and Engineering Solutions of Sandia LLC, a wholly owned subsidiary of Honeywell International Inc. for the U.S. Department of Energy's National Nuclear Security Administration under contract DE-NA0003525. This is publication SAND2018-XXXX.

References

[1] Sandia National Laboratories (SNL) (2008), Features, Events, and Processes for the Total System Performance Assessment: Methods, ANL-WIS-MD-000026. U.S. Department of Energy, Office of Civilian Radioactive Waste Management.

[2] Sandia National Laboratories (SNL) (2008), Features, Events, and Processes for the Total System Performance Assessment: Analyses, ANL-WIS-MD-000027. U.S. Department of Energy, Office of Civilian Radioactive Waste Management.

[3] W. E. Kastenberg et al. (1996), "Considerations of Autocatalytic Criticality of Fissile Materials in Geologic Repositories," Nucl. Technol., 115[3], pp. 298–310.

[4] T. Goorley et al. (2012), "Initial MCNP6 release overview," Nucl. Technol., 180[3], pp. 298–315.

[5] A. Salazar (2018), "Criticality in the far-field of a granitic repository for used nuclear fuel," University of California, Berkeley, Berkeley, CA.

[6] UC Regents (2011), TOUGH2: Transport of Unsaturated Groundwater and Heat w/ T2CG2 Solver Package. University of California.

[7] M. T. Van Genuchten (1980), "A closed-form equation for predicting the hydraulic conductivity of unsaturated soils," Soil Sci. Soc. Am. J., 44[5], pp. 892–898.

[8] F. B. Brown, W. R. Martin, G. Yesilyurt, and S. Wilderman (2012), "On-the-Fly Neutron Doppler Broadening for MCNP," Los Alamos Natl. Lab.

[9] P. N. Smith, R. M. Mason, and R. Cummings (2007), “A Model of Quasi-Steady-State Criticality Under Repository Conditions,” International Conference on Nuclear Criticality, St. Petersburg, Russia.

[10] J. S. Denton, S. J. Goldstein, P. Paviet, A. J. Nunn, R. S. Amato, and K. A. Hinrichs (2016), “A record of uranium-series transport at Nopal I, Sierra Peña Blanca, Mexico: Implications for natural uranium deposits and radioactive waste repositories,” Chemical Geology, 434, pp. 12–27.

[11] S. J. Goldstein et al. (2010), “Uranium-Series Constraints on Radionuclide Transport and Groundwater Flow at the Nopal I Uranium Deposit, Sierra Peña Blanca, Mexico,” Env. Sci. & Technol., 44[5], pp. 1579-1586.